SCIENTIFIC REPORTS

OPEN

The Role of Super-Atom Molecular Orbitals in Doped Fullerenes in a Femtosecond Intense Laser Field

Received: 4 October 2016
Accepted: 8 February 2017
Published online: 09 March 2017

Hui Xiong[1], Benoit Mignolet[2], Li Fang[3], Timur Osipov[4], Thomas J. A. Wolf[5], Emily Sistrunk[5,7], Markus Gühr[5,6], Francoise Remacle[2] & Nora Berrah[1]

The interaction of gas phase endohedral fullerene $Ho_3N@C_{80}$ with intense ($0.1–5 \times 10^{14}$ W/cm^2), short (30 fs), 800 nm laser pulses was investigated. The power law dependence of $Ho_3N@C_{80}^{q+}$, q = 1–2, was found to be different from that of C_{60}. Time-dependent density functional theory computations revealed different light-induced ionization mechanisms. Unlike in C_{60}, in doped fullerenes, the breaking of the cage spherical symmetry makes super atomic molecular orbital (SAMO) states optically active. Theoretical calculations suggest that the fast ionization of the SAMO states in $Ho_3N@C_{80}$ is responsible for the n = 3 power law for singly charged parent molecules at intensities lower than 1.2×10^{14} W/cm^2.

The behavior of atoms, molecules, nano-systems, and solids in intense laser fields[1–14] continues to reveal new dynamics. Atoms and molecules whose valence electrons can absorb several photons fall in the multiphoton ionization regime class when the Keldysh parameter $\gamma \gg 1$ ($\gamma = (I_p/2U_p)^{1/2}$, where U_p is the laser field's ponderomotive potential and I_p is the ionization potential). Those systems whose valence electrons tunnel through the potential barrier formed by the laser field and the Coulomb force, fall within the class of tunneling or over the barrier ionization, depending upon the laser field intensity[5], and with Keldysh parameter $\gamma \ll 1$[6–10].

Endohedral, or doped fullerenes, which is the topic of this Scientific Report, are intriguing systems that bridge the gap between molecular and nano-systems[15–18]. However, little is known about their structure and dynamics when excited with a strong laser field. Among their properties, electron transfer from the encaged species to the carbon cage is of special interest[15,16]. The understanding derived from the photoionization of these carbon nanomaterials enables optimizing their properties, which is relevant to their use in molecular electronics and organic photovoltaics[19]. These nanoscale systems have received attention because they can be used for applications ranging from medical usage[20] such as in imaging or drug delivery, to their employment in devices for quantum computing[21]. Our interest in investigating these systems stems from the possibility of finding novel fundamental effects making their examination a focus of fundamental research[15,16,19,22]. In fact, we show with this experimental work that doped fullerenes respond differently to intense I.R. laser fields compared to empty fullerenes. Furthermore, with our quantitative calculations, we explain in detail why their behavior is different. This work falls within the general, active topic of non-linear physics[23–33].

In recent years, non-linear physics or strong-field laser research has led to technological advances and novel phenomena[23–33]. Investigations of the behavior of molecules in short, intense laser fields[5,10,34] were extended to complex molecules, such as C_{60}, which has been challenging[35–44] due to the many electron-nuclei response it exhibits since it is a cage of 60 atoms with 240 valence electrons. The photoionization mechanisms have been found to be wavelength and pulse duration dependent[37,38,45]. For IR pulses (800 nm) of about 30 fs duration and intensities below 5×10^{13} W/cm^2, it was found that multiphoton processes dominate when ionizing C_{60}, while tunneling, and/or over-the barrier-ionization, or ionization due to induced electron re-collision[36] are not probable under these conditions. The single-active-electron (SAE) method was used to calculate the ionization of C_{60} in intense, 4×10^{13} W/cm^2, laser pulses with durations between 27 and 70 fs and for a wide range of wavelengths ranging from 395–1800 nm[39] which agreed with measurements by Shchatsinin *et al.*[40]. For a long I.R. wavelength of 1800 nm and 70 fs pulse duration, the SAE picture predicts "over the barrier" ionization for a peak intensity of

[1]Physics Department, University of Connecticut, Storrs, CT, 06269, USA. [2]Departement de Chimie, B6c, Université de Liege, B4000, Liege, Belgium. [3]Center for High Energy Density Science, University of Texas, Austin, TX, 78712, USA. [4]LCLS, National Accelerator Laboratory, Menlo Park, CA, 94025, USA. [5]Stanford PULSE Institute, SLAC National Accelerator Laboratory, Menlo Park, CA, 94025, USA. [6]Institut für Physik und Astronomie, Universität Potsdam, 14476, Potsdam, Germany. [7]Present address: Lawrence Livermoor National Laboratory, CA, USA. Correspondence and requests for materials should be addressed to N.B. (email: nora.berrah@uconn.edu)

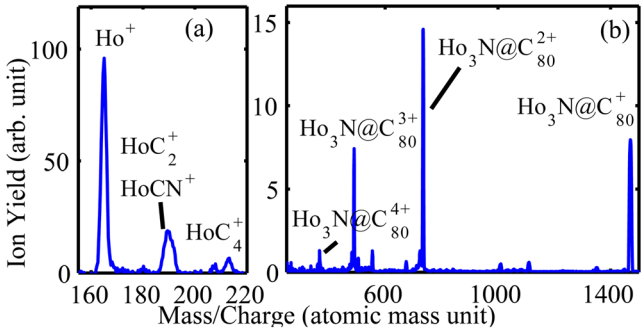

Figure 1. Mass/charge spectra of $Ho_3N@C_{80}$ ionized with laser pulses of 800 nm, 30 fs pulse duration and an intensity of 4×10^{14} W/cm^2.

10^{15} W/cm^2 leading to non-fragmented but highly charged C_{60}^{q+} (q = 1–12)[35]. At short wavelength of 355 nm, the excitation of C_{60} with 10 ns pulses leads to fragmentation by delayed ionization and C_2 emission as well as other fragments even for small intensities of about 2×10^6 W/cm^2 [43]. The use of electron spectroscopy in addition to the ion measurements raised questions for the C_{60} investigations; namely, can the ionization and fragmentation dynamics be adequately modeled in the SAE picture or should multi-electron dynamics be included[40,44]? This led to recent experimental and theoretical investigation, which concluded that both SAE and many-electron effects, are important[36].

Our motivation for this work is to contribute substantially to the field of non-linear physics by investigating increased complexity targets. We studied the photoionization of endohedral fullerenes in strong laser fields to answer the following question: Do the ionization dynamics change in fs strong laser fields for a doped fullerene compared to C_{60}, an empty fullerene and why? We use a prototype, $Ho_3N@C_{80}$, interacting with intense ($0.1–5 \times 10^{14}$ W/cm^2), short (30 fs), 800 nm laser pulses giving rise to multiply charged parent ions as well as fragment ions. We focus here on the measurement and theoretical explanation of the power law for singly ionized $Ho_3N@C_{80}$ yields, and compare our findings to C_{60} results (because pristine C_{80} is not commercially available) carried out under similar conditions[40]. Two distinct regions are present in the ion yield spectra with respect to field strength corresponding to different ionization mechanisms and power laws. For low field strengths, multiphoton ionization dominates, while for higher field strengths, tunneling and ionization over the barrier are the main ionization processes. The photoelectron spectra of endohedral fullerenes such as $Li@C_{60}$[18] or $Sc_3N@C_{80}$[46] have been measured with longer and weaker laser pulses. Although the photoionization of endohedral fullerenes was studied by other groups[13,14,18,46], none of the cases studied the role of encaged atoms or clusters in femtosecond strong laser fields. As one would expect, encaging of an atom or cluster in a carbon cage modifies the electronic structure of the fullerene, but in what way? Previously, for C_{60}, both SAMO and Rydberg states played important roles when exposed to a strong laser field[45]. Both kinds of states can be indirectly populated by vibronic coupling, but because the density of Rydberg states is higher than that of SAMO states, Rydberg state ionization in C_{60} dominates the ionization at laser intensities $>10^{13}$ W/cm^2 [45], which brought up an interesting question: do the SAMO states play a more important role in a doped fullerenes such as $Ho_3N@C_{80}$? In this work, supported by theory, we demonstrate and explain that the endohedral fullerene $Ho_3N@C_{80}$ responds differently to intense near-infrared femtosecond laser fields compared to C_{60}, because of the increased importance of the SAMO states and this is reflected by a different slope of the power law for low field strengths.

A power law corresponding to n = 5 photon was measured in C_{60} while we report here a power law of n = 3 photons for $Ho_3N@C_{80}$. In C_{60} the power law is readily understood from energetics: it takes 5 photons of 1.55 eV (800 nm) to reach the IP, 7.6 eV[40]. However, in $Ho_3N@C_{80}$ (experimental IP ~ 6.9 eV)[44,45], instead of observing a power law corresponding to 5 photons, we demonstrate below a power law corresponding to n = 3. This decrease arises from resonance-enhanced multiphoton ionization of intermediate states that promptly ionize by absorption of an extra photon. We argue these states are Super Atomic Molecular Orbital (SAMO) states similar to the ones observed in C_{60}[13,47]. The SAMO states are excited electronic states where a valence electron is promoted to a diffuse atomic-like molecular orbital. They are present in both fullerenes and characterized by very short photoionization lifetimes, in the few fs range, because of their diffuse character[11,13,48]. However, unlike in $Ho_3N@C_{80}$, the lower SAMO states of *s*, *p*, and *d* symmetry are dark states in C_{60} because of their spherical symmetry and cannot be accessed during the pulse. They can only be populated by vibronic coupling on a time scale of few tens of fs. On the contrary, SAMO states of $Ho_3N@C_{80}$ become optically active because of symmetry breaking induced by the inclusion of Ho_3N inside the symmetric but non-spherical C_{80} fullerene cage. We show below that the optically active SAMO states in $Ho_3N@C_{80}$ can be accessed by the absorption of 3 photons during the pulse. Upon absorption of these 3 photons, the SAMO states of $Ho_3N@C_{80}$ almost instantaneously photoionize, which makes photoexcitation the rate limiting step and explains the n = 3 observed power law. Note that the only theoretically calculated IPs available in the literature are 6.88 eV for $Sc_3N@C_{80}$[49] and 6.93 eV for $Lu_3N@C_{80}$[50]. All of these values are very close to 6.84 eV for the C_{80} molecule[51].

The experiment was performed using an ion velocity map imaging (VMI) spectrometer used in the time of flight (TOF) mode and details are available in the Supplementary information (S.I.) and in refs 52 and 53. The ion-mass spectrum of $Ho_3N@C_{80}$ at 800 nm obtained at a laser intensity of 4×10^{14} W/cm^2 and 30 fs pulse duration is shown in Fig. 1. We observe parent ions up to $Ho_3N@C_{80}^{4+}$ although the statistics is low for $Ho_3N@C_{80}^{4+}$.

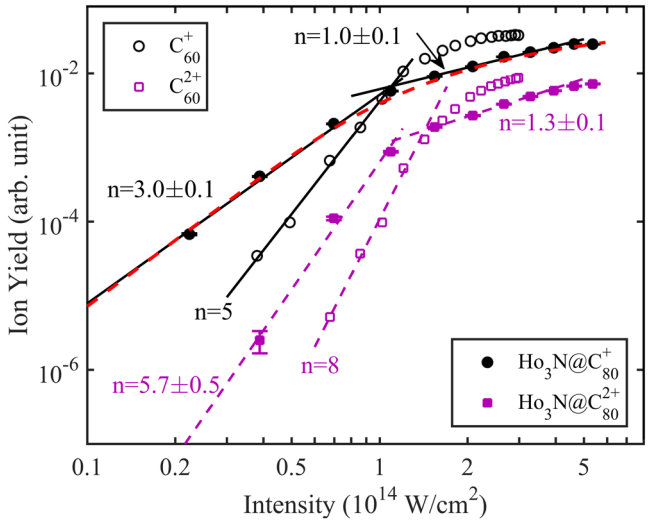

Figure 2. Comparison of the ion yield dependence on peak intensity for the ionization of $Ho_3N@C_{80}^{q+}$ (q = 1, 2) (filled symbols) and C_{60}^{q+} (q = 1, 2) (open symbols). The $Ho_3N@C_{80}^{q+}$ results are extracted from data in Fig. 1 and the yields of $Ho_3N@C_{80}$ with a charge q = 1 is multiplied by 5. The C_{60} data are from ref. 40 and the C_{60}^{+} yield was multiplied by 2 for clarity.

Charge state q	q = 1+	q = 2+
C_{60}	5	8
$Ho_3N@C_{80}$	3.0 (±0.1)	5.7 (±0.5)

Table 1. Measured power laws for $HoN_3@C_{80}$ and for C_{60}[40] ion charge states.

We also observed Ho-based molecular fragment ions: HoC_2^+, $HoCN^+$, and HoC_4^+, as well as atomic Ho^+ ions (the most abundant) created by bond breaking and bond forming. In this report, we focus on the parent ion yield power laws.

In this work, we investigated the dependence of $Ho_3N@C_{80}^{q+}$ (q = 1–2) yields as a function of the peak laser intensity and our results are shown in Fig. 2. We find that the yields for $Ho_3N@C_{80}$ ions follow the power law $Y = I^n$ as a function of laser field intensity I[40, 42]. To determine the power laws, linear fits were applied to the experimental ion yields using a least-squares fit for intensities higher than 1.2×10^{14} W/cm^2. Then, the rest of the data, which significantly deviated from the power law at high intensity, were fit by lines with different slopes. The fitting errors for the $Ho_3N@C_{80}$ ions are shown in Fig. 2. The observed slopes for q = 1, 2 at lower intensities ($<1.2 \times 10^{14}$ W/cm^2) are 3.0 ± 0.1 and 5.7 ± 0.5, respectively and are summarized in Table 1. The intensity at the cross point of the two slopes is defined as the saturation intensity[42]. As the intensity increases beyond saturation for each of the ion species, the yields start to follow an almost linear trend with a shallower slope, indicating that the ionization saturation has been reached[39, 54].

To check our findings, we performed a simulation of the ion yield of singly charged $Ho_3N@C_{80}$ through three-photon resonant ionization, taking focal volume averaging into account. The generalized 3-photon cross section σ_3 is defined by the ionization probability per unit detection volume, $W(t) = \sigma_3(I/h\nu)^3$. Experimental parameters used in the simulation are laser focal waist (20 μm), pulse duration (30 fs), and diameter of the molecular beam (4 mm). The yield of singly charged $Ho_3N@C_{80}$ was obtained by integrating the ionization rate in the interaction region. By adjusting the cross section σ_3, we obtained a reasonable result shown as the red dashed line in Fig. 2. We note that within the accuracy of the parameters, the result of the simulation does not significantly change.

The strong field ionization (SFI) mechanisms of $Ho_3N@C_{80}$ with the current IR laser conditions include multiphoton, tunneling, and over the barrier ionization, based on our computation of the barrier lowering induced by the strong field. We find that the multiphoton ionization mechanism dominates at low laser intensities ($<5 \times 10^{13}$ W/cm^2, corresponding to $\gamma > 1.0$) and tunnel ionization[5] dominates at high laser intensities ($>10^{14}$ W/cm^2, corresponding to $\gamma < 0.75$). In the intermediate region, where γ varies between 1.0 and 0.75, there is a complex interplay among the multiphoton, tunneling, over the barrier mechanisms as well as ionization saturation.

In Fig. 2, we compare power law slopes for the doped fullerene results with that of C_{60}. The wavelength of the laser used in both experiments was 800 nm, while the laser pulse duration in the C_{60} experiment was 27 fs, close to the 30 fs used in the current experiment and within the error bar. The error bar on the laser intensity was 15%. As can be seen from Table 1, the slopes of power law are substantially higher for the ionization of C_{60} compared to $Ho_3N@C_{80}$.

Electronic structure computations were performed to elucidate the power law difference between C_{60} and $Ho_3N@C_{80}$. The equilibrium geometry of the $Ho_3N@C_{80}$'s isomers was computed at the DFT/PBE0[55] level (see

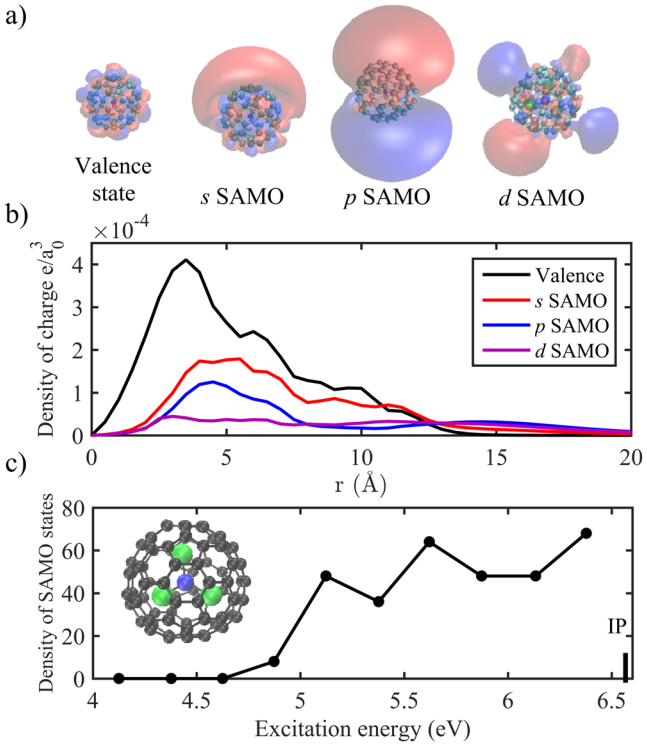

Figure 3. (**a**) Dyson orbitals of a typical valence state, *s* SAMO, *p* SAMO and *d* SAMO states of $Ho_3N@C_{80}$ with an isocontour of 0.002|e|/Å. (**b**) Charge density of the Dyson orbitals of panel a. (**c**) Density of SAMO states as a function of the excitation energy. The electronic states and Dyson orbitals have been computed in TDDFT at the LC-BLYP/6–31G(d) + ECP56MWB/7s6p5d for Ho + Bq (6–31(6+)G(d)) level for $Ho_3N@C_{80}$'s lowest energy isomer shown in the inset.

computational details in S.I.). The starting geometries were obtained by adding the Ho_3N complex inside each of the six C_{80} isomers. The most stable isomer has a slightly triangular C_{80} cage with the nitrogen atom localized at the center, and a Ho-N bond length of 2.06 Å (the shortest compared to the other stable isomers). The inclusion of the Ho_3N complex in the cage induces a significant lowering of the symmetry. The bare C_{80} belongs to the D_{5h} point group while $Ho_3N@C_{80}$ exhibits an approximate C_2 symmetry (see S.I. for details). The computed vertical ionization potential (IP) of the lowest energy isomer is 6.54 eV, which is close to the experimental IP of the C_{80} fullerene (6.84 eV)[51]. The ionization potentials of the other isomers are significantly lower, see Table S1 in the S.I. In the following discussion, we only refer to the lowest energy isomer. Similar doped fullerenes such as $Y_3N@C_{80}$[56] and $Lu_2CeN@C_{80}$[50] exhibit a triangular cage and a similar ionization potential.

The electronic structures of the 250 lowest SAMO and valence excited electronic states of $Ho_3N@C_{80}$'s most stable isomer were computed in TDDFT with the LC-BLYP functional[57,58] (see computational details in the S.I., note that no Rydberg states are present in the band because their computation requires a larger basis of atomic orbitals that includes more highly diffuse basis functions). Particular attention was given to the excited states coined as super-atom-molecular orbital (SAMO) states[47]. SAMO excited states were first discovered for the case of fullerenes on metal surfaces[47]. They are diffuse hydrogen-like orbitals resulting from the shallow potential present at the center of hollow systems such as fullerenes[11,13,14,47]. The SAMO excited states are different from other Rydberg states because of the significant electronic density localized inside the carbon cage as shown in Fig. 3(a,b). They were called SAMOs because for C_{60}, they exhibit the spherical harmonic shapes *s*, *p*, or *d* atomic orbital symmetry[47]. For C_{60} adsorbed on surfaces[47] and in the gas phase[13,14], sharp bands of *s*, *p*, and *d* SAMO's were identified[48]. Due to the symmetry breaking induced by the insertion of the Ho_3N inside the cage, in the case of $Ho_3N@C_{80}$, there is a broad manifold of excited states with delocalized diffuse orbitals of type *s*, *p*, and *d*, analogous to the C_{60}'s SAMO states. For this reason, we also named these states SAMO but they are not pure *s*, *p*, or *d* SAMO states as in C_{60} because the presence of Ho_3N induces a mixing of the SAMO states with the valence states as shown in Fig. 3a. Moreover, unlike those of C_{60}, the SAMO states in $Ho_3N@C_{80}$ are optically active because of the symmetry breaking of the cage. For instance, the transition dipole moment between the ground state and the *s* SAMO state is close to zero in C_{60} and C_{80} while it is 0.66au in $Ho_3N@C_{80}$ (Table 2).

As can be seen in Fig. 3(c), the number of SAMO states increases with the excitation energy and reaches a maximum at about 5.75 eV. The lowest SAMO state of $Ho_3N@C_{80}$ has an excitation energy of 4.98 eV and a non-zero transition dipole moment, like all the SAMO states, so that it can be directly accessed from the ground state during the pulse. Its excitation energy corresponds to 3.2 photons but the laser pulse has a FMHW width of 0.15 eV (per photon) so that this state can directly be accessed through 3-photon absorption during the pulse.

	Excitation energy(eV)	Photoionization lifetime (fs)		μ_{trans} (au)		
		10^{13} W/cm^2	10^{14} W/cm^2	$Ho_3N@C_{80}$	C_{60}	C_{80}
Valence (ES 67)	4.25	351.03	39.00	1.19	1.55	1.47
s SAMO (ES 100)	4.98	2.00	0.22	0.66	0.00	0.02
p SAMO (ES 116)	5.23	1.49	0.13	0.69	0.00	0.30
d SAMO (ES 145)	5.60	1.56	0.17	0.49	0.00	0.29

Table 2. Computed binding energies, photoionization lifetimes (in fs) for a field intensity of 10^{13} and 10^{14} W/cm^2 and transition dipole moments (μ_{trans}) between the ground and excited states shown in Fig. 3. The photoionization lifetimes are computed for the ionization of an electron with a kinetic energy of 0.2 eV. For comparison, the computed transition dipole moments of the valence (with an excitation energy around 4.25 eV), *s*, *p* and *d* SAMO states are also given for C_{60} and C_{80}.

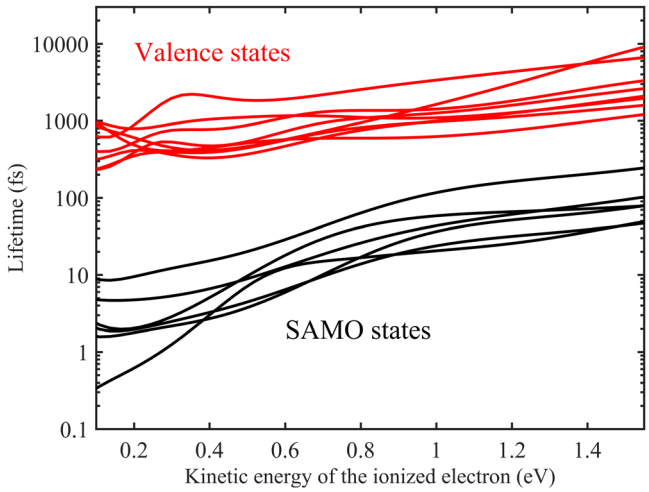

Figure 4. Photoionization lifetime (field intensity of 10^{13} W/cm^2) for a set of representative SAMO and valence states, plotted as a function of the kinetic energy of electron ionized from the SAMO or valence states. Amongst the valence states, some are isoenergetic with the SAMO states (see S.I. for details).

Once the SAMO states are photoexcited during the pulse, they can promptly ionize due to their short photoionization lifetime (i.e. the time it takes to photoionize 63% of the population). The lifetimes, that are inversely proportional to the square modulus of the photoionization coupling elements **V**, have been computed for the 250 lowest excited states of $Ho_3N@C_{80}$ using the formalism described in references[59,60].

$$\mathbf{V}(\varepsilon) = E_0\langle\phi^{Dyson}|\mathbf{E}\cdot\mathbf{r}|\chi^{electron}(\varepsilon)\rangle \quad (1)$$

Here, E_0 is the electric field amplitude, **E** the electric field polarization vector, $\chi^{electron}(\varepsilon)$ the wavefunction of the ionized electron and ϕ^{Dyson} is the Dyson orbital[11,48,61,62], which is the overlap between the neutral and cationic wavefunctions. The Dyson orbitals provide a correlated view of the wave function of the ionized electron and play a crucial role in the interpretation of photoelectron lifetimes and angular distributions. We find that the Dyson orbitals of the SAMO states (Fig. 3a) in $Ho_3N@C_{80}$ have a small valence character and are distorted compared to the ones of the spherical C_{60} fullerene due in part to the loss of symmetry of the slightly triangular C_{80} cage but primarily to the inclusion of Ho_3N inside the C_{80} cage (Fig. 4a). The presence of Ho_3N drastically changes the amount of charge density of the Dyson orbital inside the cage compared to that of the bare C_{60}. For instance, in C_{60} the charge density of the *s* SAMO is maximal at the center of cage (r = 0) while in $Ho_3N@C_{80}$, the nitrogen lies at the center of the cage so the *s* SAMO charge density is zero at r = 0 and then increases.

In Eq. 1, the Coulomb interaction between the fullerene cage and the departing electron is neglected, which can affect the momentum of the leaving electron, especially for low kinetic energy electrons. Within this approximation, the wavefunction of the electron is described by an orthogonalized plane wave. Previous work on C_{60}

showed that the relative photoionization intensities of SAMO states computed using this approximation were in good agreement with the experimental values[63], which suggests a minor role of the Coulomb interactions for kinetic energy of the photoelectrons ranging from 0.2 to 1.55 eV. From Eq. 1, we can readily compute the lifetimes that are inversely proportional to the field intensity and to the dipole coupling between the Dyson orbital and the ionized electron. Due to their simple hydrogenoid shape, the SAMO states have a large dipole coupling compared to the isoenergetic valence excited states[48], which leads to lifetimes several orders of magnitude smaller than the ones of the isoenergetic valence excited states (see Table 2 and Fig. 4(c)). For a field intensity of 10^{13} W/cm^2, the SAMO states have lifetimes on the order of a femtosecond, which is short compared to several hundreds of fs for the valence states. When the SAMO states are populated, they promptly ionize, unlike the valence states that slowly ionize during the pulse. The limiting rate determining step for the SAMO states is their photoexcitation while for the valence states it is their photoionization. The SAMO state lifetimes strongly depend on the kinetic energy of the ionized electron and increase faster than the valence state lifetimes. Nevertheless, even for a kinetic energy of 1.55 eV (≈one IR photon), the SAMO states still ionize on average 35 times faster than the valence states.

For low laser intensities, the slope of the power law in the photoionization region is expected to be the number of photon necessary to ionize the ground state, as it is the case in C_{60} and which should be 5 for $Ho_3N@C_{80}$. However, the observed value of "n" is found to be 3 (Table 1), which indicates there are intermediates resonant states[64] in the photoionization process. These states could be valence or SAMO excited states because they both are optically active (Table 2) and can therefore be transiently populated during the pulse. However, the SAMO states have lifetimes around two orders of magnitude shorter than the valence states so if both type of states are populated during the pulse, ionization would mainly come from the SAMO states. Thus the SAMO states act as fast ionizing intermediate resonant states, which affects the power law, as the rate-determining step is now the photoexcitation process to the SAMO states instead of the photoionization as is the case of C_{60}. Such a process does not occur in C_{60} because the SAMO states are not optically active so they cannot be promptly excited from the ground state by direct multiphoton excitation. They can only be populated indirectly by vibronic coupling to isoenergetic optically active valence states[14], which takes several tens of fs. Therefore, the transient population in the SAMO states during the pulse is larger in $Ho_3N@C_{80}$ than in C_{60}, and so is the ion yield as shown in Fig. 2.

It is known that strong laser fields can induce vibrations in C_{60} ions[65]. Vibrational excitation and significant geometric distortion[66] may shift the ionization potential of C_{60}. However, the laser intensity used in this report is much smaller than the one used in reference[65]. It is thus unlikely that the ionization of the parent molecules was affected by the ionization potential change due to the small vibrational energy accumulated during the laser pulse[65].

For laser intensities higher than 10^{14} W/cm^2, where $\gamma < 0.75$, ionization over the barrier and tunnel ionization are the main mechanisms. Therefore, the ion yields of $Ho_3N@C_{80}$ and C_{60} are of the same order because it does not depend anymore on the photoexcitation of the SAMO states during the pulse. In the intermediate region, for field intensity ranging from $5 \times 10^{13} - 1 \times 10^{14}$ W/cm^2, both multiphoton and over the barrier ionization mechanisms coexist. The change of mechanisms is reflected in the ion yield that reaches saturation around 9×10^{13} W/cm^2 for $Ho_3N@C_{80}$. At this field intensity, we computed a lowering of the IP (second order stark shift) of 1.9 eV, which means that some of the valence states with a slightly higher binding energy than the lowest SAMO states can ionize over the barrier. These states can be accessed by one photon less than the SAMO states and they have transition dipole moments from the ground state up to 5 times larger, which can explain the saturation observed.

In summary, this experimental and theoretical work examined the interaction of a complex system, an endohedral fullerene with short, intense laser pulses, revealing fundamental differences compared to the case of an empty cage such as C_{60}. We explain quantitatively that the clear signature difference is directly linked to the role of SAMO states in both molecules. Although the dominant photoionization mechanism is multiphoton ionization for both fullerenes, the measurement of the laser intensity power law dependence, I^n, of the singly and doubly charged $Ho_3N@C_{80}$ molecule was interestingly found to be different compared to C_{60}. This difference was explained in detail for $Ho_3N@C_{80}^+$ using TDDFT calculations, revealing that SAMO states act as intermediate resonances with larger photoionization widths compared to isoenergetic valence excited states. Both the C_{60} and $Ho_3N@C_{80}$ SAMO states have photoionization lifetimes of the order of the fs for field intensity higher than 10^{13} W/cm^2. The optically active $Ho_3N@C_{80}$ states can quickly ionize during the 30 fs pulses because they are populated, unlike C_{60}'s SAMO states that can only be populated indirectly by vibronic coupling. The SAMO states of $Ho_3N@C_{80}$ can be optically accessed during the short pulse duration because of their non-zero transition dipole moments, resulting from the symmetry breaking. This experimental and theoretical work demonstrated that the photoionization of a doped fullerene in strong field has a clear signature difference compared to the case of empty C_{60}[13,14] and of C_{60} adsorbed on surfaces[47]. Furthermore, this work has revealed that an encapsulated molecule inside a cage breaks the fullerene symmetry leading to different photo-dynamics and this result should be general for these nano-systems excited under similar conditions. In addition to contributing new knowledge to the active topic of strong field research, our work on doped fullerenes connects to other areas of science since it impacts the understanding of these nano-systems, which have shown the promise to be used in the design of molecular electronics and optoelectronics materials[47,67,68] as well as used for applications ranging from medical usage[20] such as in imaging or drug delivery, and in devices for quantum computing[21].

References

1. Delone, N. B. & Vladimir, P. K. Tunneling and barrier-suppression ionization of atoms and ions in a laser radiation field. *Phys. Usp* **41**, 469 (1998).
2. Krause, J. L., Schafer, K. J. & Kulander, K. C. Calculation of photoemission from atoms subject to intense laser fields. *Phys. Rev. A* **45**, 4998–5010 (1992).
3. Pullen, M. G. *et al.* Imaging an aligned polyatomic molecule with laser-induced electron diffraction. *Nat. Commun.* **6**, 7262 (2015).
4. Vampa, G. *et al.* Linking high harmonics from gases and solids. *Nature* **522**, 462–464 (2015).

5. Lezius, M. *et al.* Nonadiabatic Multielectron Dynamics in Strong Field Molecular Ionization. *Phys. Rev. Lett.* **86**, 51–54 (2001).
6. Keldysh, L. V. Ionization in the field of a strong electromagnetic wave. *Sov. Phys. JETP* **20**, 1307–1314 (1965).
7. DeWitt, M. J. & Levis, R. J. Calculating the Keldysh adiabaticity parameter for atomic, diatomic, and polyatomic molecules. *J. Chem. Phys.* **108**, 7739–7742 (1998).
8. Reitsma, G. *et al.* Femtosecond laser induced ionization and dissociation of gas-phase protonated leucine enkephalin. *Int. J. Mass spectrom.* **365–366**, 365–371 (2014).
9. Scarborough, T. D., Foote, D. B. & Uiterwaal, C. J. G. J. Ultrafast resonance-enhanced multiphoton ionization in the azabenzenes: Pyridine, pyridazine, pyrimidine, and pyrazine. *J. Chem. Phys.* **136**, 054309 (2012).
10. Zhao, S.-F., Le, A.-T., Jin, C., Wang, X. & Lin, C. D. Analytical model for calibrating laser intensity in strong-field-ionization experiments. *Phys. Rev. A* **93**, 023413 (2016).
11. Mignolet, B., Kûs, T. & Remacle, F. In *Imaging and Manipulating Molecular Orbitals: Proceedings of the 3rd AtMol International Workshop, Berlin 24–25 September 2012* (eds Leonhard, Grill & Christian, Joachim) 41–54 (Springer Berlin Heidelberg, 2013).
12. Leone, S. R. *et al.* What will it take to observe processes in 'real time'? *Nat. Photon* **8**, 162–166 (2014).
13. Johansson, J. O., Henderson, G. G., Remacle, F. & Campbell, E. E. B. Angular-resolved Photoelectron Spectroscopy of Superatom Orbitals of Fullerenes. *Phys. Rev. Lett.* **108**, 173401 (2012).
14. Johansson, J. O. & Campbell, E. E. B. Probing excited electronic states and ionisation mechanisms of fullerenes. *Chem. Soc. Rev.* **42**, 5661–5671 (2013).
15. Popov, A. A. & Dunsch, L. Hindered cluster rotation and ^{45}Sc hyperfine splitting constant in distonoid anion radical $Sc_3N@C_{80}^-$, and spatial spin-charge separation as a general principle for anions of endohedral fullerenes with metal-localized lowest unoccupied molecular orbitals. *J. Am. Chem. Soc.* **130**, 17726–17742 (2008).
16. Rodriguez-Fortea, A., Balch, A. L. & Poblet, J. M. Endohedral metallofullerenes: a unique host-guest association. *Chem. Soc. Rev.* **40**, 3551–3563 (2011).
17. Gromov, A., Krawez, N., Lassesson, A., Ostrovskii, D. I. & Campbell, E. E. B. Optical properties of endohedral $Li@C_{60}$. *Current Applied Physics* **2**, 51–55 (2002).
18. Lassesson, A. *et al.* A femtosecond laser study of the endohedral fullerenes $Li@C_{60}$ and $La@C_{82}$. *Eur. Phys. J. D* **34**, 205 (2005).
19. Wang, Y., Yamachika, R., Wachowiak, A., Grobis, M. & Crommie, M. F. Tuning fulleride electronic structure and molecular ordering via variable layer index. *Nat. Mater.* **7**, 194–197 (2008).
20. Melanko, J. B., Pearce, M. E. & Salem, A. K. In *Nanotechnology in Drug Delivery* (eds Melgardt M., de Villiers, Pornanong, Aramwit & Glen S., Kwon) 105–127 (Springer New York, 2009).
21. Harneit, W. *et al.* Room Temperature Electrical Detection of Spin Coherence in C_{60}. *Phys. Rev. Lett.* **98**, 216601 (2007).
22. Heath, J. R. *et al.* Lanthanum complexes of spheroidal carbon shells. *J. Am. Chem. Soc.* **107**, 7779–7780 (1985).
23. Corkum, P. B. Plasma perspective on strong field multiphoton ionization. *Phys. Rev. Lett.* **71**, 1994–1997 (1993).
24. Hart, N. A. *et al.* Intensity-resolved above-threshold ionization of xenon with short laser pulses. *Phys. Rev. A* **89**, 053414 (2014).
25. Chini, M., Zhao, K. & Chang, Z. The generation, characterization and applications of broadband isolated attosecond pulses. *Nat. Photon* **8**, 178–186 (2014).
26. Krausz, F. & Stockman, M. I. Attosecond metrology: from electron capture to future signal processing. *Nat. Photon* **8**, 205–213 (2014).
27. Paasch-Colberg, T. *et al.* Solid-state light-phase detector. *Nat. Photon* **8**, 214–218 (2014).
28. Beck, A. R., Neumark, D. M. & Leone, S. R. Probing ultrafast dynamics with attosecond transient absorption. *Chem. Phys. Lett.* **624**, 119–130 (2015).
29. Torlina, L. *et al.* Interpreting attoclock measurements of tunnelling times. *Nat. Phys* **11**, 503–508 (2015).
30. Ghimire, S. *et al.* Observation of high-order harmonic generation in a bulk crystal. *Nat. Phys* **7**, 138–141 (2011).
31. Schubert, O. *et al.* Sub-cycle control of terahertz high-harmonic generation by dynamical Bloch oscillations. *Nat. Photon* **8**, 119–123 (2014).
32. Ulstrup, S. *et al.* Ultrafast Dynamics of Massive Dirac Fermions in Bilayer Graphene. *Phys. Rev. Lett.* **112**, 257401 (2014).
33. Hickstein, D. D. *et al.* Mapping Nanoscale Absorption of Femtosecond Laser Pulses Using Plasma Explosion Imaging. *ACS Nano* **8**, 8810–8818 (2014).
34. Strohaber, J. *et al.* Intensity-resolved ionization yields of aniline with femtosecond laser pulses. *Phys. Rev. A* **84**, 063414 (2011).
35. Bhardwaj, V. R., Corkum, P. B. & Rayner, D. M. Internal laser-induced dipole force at work in C_{60} molecule. *Phys. Rev. Lett.* **91**, 203004 (2003).
36. Huismans, Y. *et al.* Macro-atom versus many-electron effects in ultrafast ionization of C_{60}. *Phys. Rev. A* **88**, 013201 (2013).
37. Campbell, E. E. *et al.* From above threshold ionization to statistical electron emission: the laser pulse-duration dependence of C_{60} photoelectron spectra. *Phys. Rev. Lett.* **84**, 2128 (2000).
38. Kjellberg, M. *et al.* Momentum-map-imaging photoelectron spectroscopy of fullerenes with femtosecond laser pulses. *Phys. Rev. A* **81**, 023202 (2010).
39. Jaroń-Becker, A., Becker, A. & Faisal, F. H. M. Single-active-electron ionization of C_{60} in intense laser pulses to high charge states. *J. Chem. Phys.* **126**, 124310 (2007).
40. Shchatsinin, I. *et al.* C_{60} in intense short pulse laser fields down to 9 fs: excitation on time scales below e-e and e-phonon coupling. *J. Chem. Phys.* **125**, 194320 (2006).
41. Campbell, E. E. B., Hoffmann, K., Rottke, H. & Hertel, I. V. Sequential ionization of C_{60} with femtosecond laser pulses. *J. Chem. Phys.* **114**, 1716 (2001).
42. Tchaplyguine, M. H. K. *et al.* Ionization and fragmentation of C_{60} with sub-50 fs laser pulses. *J. Chem. Phys.* **112**, 2781 (2000).
43. Lebeault, M.-A. *et al.* Decay of C_{60} by delayed ionization and C_2 emission: Experiment and statistical modeling of kinetic energy release. *J. Chem. Phys.* **137**, 054312 (2012).
44. Li, H. *et al.* Coherent Electronic Wave Packet Motion in C_{60} Controlled by the Waveform and Polarization of Few-Cycle Laser Fields. *Phys. Rev. Lett.* **114**, 123004 (2015).
45. Li, H. *et al.* Transition from SAMO to Rydberg State Ionization in C_{60} in Femtosecond Laser Fields. *The Journal of Physical Chemistry Letters* **7**, 4677–4682 (2016).
46. Johansson, J. O. *et al.* Hot electron production and diffuse excited states in C_{70}, C_{82}, and $Sc_3N@C_{80}$ characterized by angular-resolved photoelectron spectroscopy. *J. Chem. Phys.* **139**, 084309 (2013).
47. Feng, M., Zhao, J. & Petek, H. Atomlike, Hollow-Core–Bound Molecular Orbitals of C_{60}. *Science* **320**, 359–362 (2008).
48. Mignolet, B., Johansson, J. O., Campbell, E. E. B. & Remacle, F. Probing Rapidly-Ionizing Super-Atom Molecular Orbitals in C_{60}: A Computational and Femtosecond Photoelectron Spectroscopy Study. *Chem. Phys. Chem.* **14**, 3332–3340 (2013).
49. Campanera, J. *Theoretical Characterisation of Metallofullerenes* PhD thesis, Rovira i Virgili University (2004).
50. Zhang, L. *et al.* An endohedral redox system in a fullerene cage: the Ce based mixed-metal cluster fullerene $Lu_2CeN@C_{80}$. *PCCP* **12**, 7840–7847 (2010).
51. Zimmerman, J. A., Eyler, J. R., Bach, S. B. H. & McElvany, S. W. "Magic number" carbon clusters: Ionization potentials and selective reactivity. *J. Chem. Phys.* **94**, 3556–3562 (1991).
52. Pešić, Z. D., Rolles, D., Dumitriu, I. & Berrah, N. Fragmentation dynamics of gas-phase furan following K-shell ionization. *Phys. Rev. A* **82**, 013401 (2010).
53. Berrah, N. *et al.* Femtosecond X-ray-induced fragmentation of fullerenes. *J. Mod. Opt* **63**, 390–401 (2016).

54. Hankin, S. M., Villeneuve, D. M., Corkum, P. B. & Rayner, D. M. Intense-field laser ionization rates in atoms and molecules. *Phys. Rev. A* **64**, 013405 (2001).
55. Adamo, C. & Barone, V. Toward reliable density functional methods without adjustable parameters: The PBE0 model. *J. Chem. Phys.* **110**, 6158–6170 (1999).
56. Popov, A. A., Zhang, L. & Dunsch, L. A Pseudoatom in a Cage: Trimetallofullerene $Y_3@C_{80}$ Mimics $Y_3N@C_{80}$ with Nitrogen Substituted by a Pseudoatom. *ACS Nano* **4**, 795–802 (2010).
57. Becke, A. D. Density-functional exchange-energy approximation with correct asymptotic behavior. *Phys. Rev. A* **38**, 3098–3100 (1988).
58. Iikura, H., Tsuneda, T., Yanai, T. & Hirao, K. A long-range correction scheme for generalized-gradient-approximation exchange functionals. *J. Chem. Phys.* **115**, 3540–3544 (2001).
59. Mignolet, B., Levine, R. D. & Remacle, F. Localized electron dynamics in attosecond-pulse-excited molecular systems: Probing the time-dependent electron density by sudden photoionization. *Phys. Rev. A* **86**, 053429 (2012).
60. Seabra, G. M., Kaplan, I. G., Zakrzewski, V. G. & Ortiz, J. V. Electron propagator theory calculations of molecular photoionization cross sections: The first-row hydrides. *J. Chem. Phys.* **121**, 4143–4155 (2004).
61. Melania Oana, C. & Krylov, A. I. Dyson orbitals for ionization from the ground and electronically excited states within equation-of-motion coupled-cluster formalism: Theory, implementation, and examples. *J. Chem. Phys.* **127**, 234106 (2007).
62. Patchkovskii, S., Zhao, Z., Brabec, T. & Villeneuve, D. M. High harmonic generation and molecular orbital tomography in multielectron systems. *J. Chem. Phys.* **126**, 114306 (2007).
63. Bohl, E. *et al.* Relative Photoionization Cross Sections of Super-Atom Molecular Orbitals (SAMOs) in C_{60}. *The Journal of Physical Chemistry A* **119**, 11504–11508 (2015).
64. Koch, M., Wolf, T. J. A. & Gühr, M. Understanding the modulation mechanism in resonance-enhanced multiphoton probing of molecular dynamics. *Phys. Rev. A* **91**, 031403 (2015).
65. Nakai, K. *et al.* Ab initio molecular dynamics and wavepacket dynamics of highly charged fullerene cations produced with intense near-infrared laser pulses. *Chem. Phys.* **338**, 127–134 (2007).
66. Kim, S. G. & Tománek, D. Melting the fullerenes: A molecular dynamics study. *Phys. Rev. Lett.* **72**, 2418–2421 (1994).
67. Ross, R. B. *et al.* Endohedral fullerenes for organic photovoltaic devices. *Nat. Mater.* **8**, 208–212 (2009).
68. Huang, T. *et al.* Superatom orbitals of $Sc_3N@C_{80}$ and their intermolecular hybridization on Cu(110)−(2 × 1)-O surface. *Phys. Rev. B* **81**, 085434 (2010).

Acknowledgements

This work was funded by the Department of Energy, office of Science, Basic Energy Sciences (BES), Division of Chemical Sciences, Geosciences, and Biosciences under grants Nos DE-SC0012376 and DE-SC0012628. FR and BM acknowledge support from the Fonds National de la Recherche Scientifique, Belgium. Computational resources have been provided by the Consortium des Équipements de Calcul Intensif (CÉCI), funded by the Fonds de la Recherche Scientifique de Belgique (F.R.S.-FNRS) under Grant No. 2.5020.11. LF acknowledges the support by Defense Advanced Research Project Agency Contract 12-63-PULSE-FP014, and by National Nuclear Security Administration Cooperative Agreement DE-NA0002008. TW thanks the German National Academy of Sciences Leopoldina for a fellowship (LPDS2013-14). We thank Nora Kling for her help with the manuscript.

Author Contributions

N.B. conceived the project and H.X. coordinated and lead the experiment. H.X., M.G., T.O., and L.F. prepared the fullerene molecular source. T.O. set up the spectrometer with H.X., L.F., T.W., and E.S. and they all carried out the experiment. H.X. analyzed the experimental data and prepared the figures. F.R. and B.M. developed the theoretical model. N.B., F.R., B.M. co-wrote the paper with the contribution of all co-authors.

Additional Information

Supplementary information accompanies this paper at doi:10.1038/s41598-017-00124-9

Competing Interests: The authors declare that they have no competing interests.

Publisher's note: Springer Nature remains neutral with regard to jurisdictional claims in published maps and institutional affiliations.